

Cite this: DOI: 00.0000/xxxxxxxxxx

Teacher-student training improves accuracy and efficiency of machine learning inter-atomic potentials[†]

Sakib Matin^{*a}, Alice Allen^{a,b}, Emily Shinkle^c, Aleksandra Pachaliev^d, Galen T. Craven^a, Benjamin Nebgen^a, Justin Smith^e, Richard Messerly^a, Ying Wai Li^b, Sergei Tretiak^{a,b,f}, Kipton Barros^{a,b}, and Nicholas Lubbers^c

Received Date

Accepted Date

DOI: 00.0000/xxxxxxxxxx

Machine learning inter-atomic potentials (MLIPs) are revolutionizing the field of molecular dynamics (MD) simulations. Recent MLIPs have tended towards more complex architectures trained on larger datasets. The resulting increase in computational and memory costs may prohibit the application of these MLIPs to perform large-scale MD simulations. Here, we present a teacher-student training framework in which the latent knowledge from the teacher (atomic energies) is used to augment the students' training. We show that the light-weight student MLIPs have faster MD speeds at a fraction of the memory footprint compared to the teacher models. Remarkably, the student models can even surpass the accuracy of the teachers, even though both are trained on the same quantum chemistry dataset. Our work highlights a practical method for MLIPs to reduce the resources required for large-scale MD simulations.

1 Introduction

Molecular Dynamics (MD)¹ is ubiquitous in chemistry,² materials science,³ and drug discovery⁴ as well as other fields. Accurate chemical and thermodynamic properties derived from MD rely on accurate inter-atomic potentials, which parameterize the many-body interactions present between atoms.^{1,5} Simulation scales may vary greatly depending on the questions of interest and available resources, and there is a persistent need for greater model efficiency. Traditional classical potentials are very fast, making it possible to perform large-scale simulations of billions of atom,⁶ or to perform hundreds of millions of integration time-steps for small systems. Recently, there is great demand for interatomic potentials that are more accurate via machine learning models that are trained to reference quantum mechanical force calculations. Here, the goals of efficiency and accuracy can be in conflict. Our paper is concerned with techniques for improving the efficiency of the inter-atomic potential *without* sacrificing accuracy.

The gold-standard for computational chemistry is *ab initio*

molecular dynamics, which uses quantum chemistry (QC) methods for accurately calculating inter-atomic forces from first principles.^{7,8} However, the often prohibitive computational cost of QC methods, and its rapid growth with system size, limits the size of the systems that can be simulated. Machine learning inter-atomic potentials (MLIPs)^{9–13} can be trained on QC datasets to map from an atomic configuration to energy and forces. MLIPs can achieve the chemical accuracy (error < 1kcal/mol) of QC simulations¹⁴ at drastically reduced computational costs. Most MLIPs achieve linear scaling with system size by utilizing the approximation that the total predicted energy can be decomposed as a sum of spatially local atom-wise or pair-wise contributions.^{11,12,15,16} MLIPs have seen explosive growth and have been successfully applied to predicting potential energy surfaces,^{17–25} with extensions to a variety of quantities, such as charges,^{26–30} and more.^{31–35} However, MLIPs only mitigate the cost of QC—they do not eliminate it. Generating training data for MLIPs is costly due to the steep scaling of QC methods in system size N , e.g., $\mathcal{O}(N^7)$ at the CCSD(T) level of theory.⁷ Therefore any approach which uses data more efficiently can potentially reduce the overall computational costs of MLIPs.

Furthermore, a recent trend in the field is the significant effort to construct foundation model MLIPs^{36–38} with broad chemical coverage,³⁹ inspired by the success of large pre-trained models in natural language processing.⁴⁰ Foundation MLIPs,⁴¹ which may be parameterized by up to 10^9 fitting parameters,⁴² have high computational and memory requirements.⁴³ These increasing computational and memory costs compared to classical force

^a Theoretical Division, Los Alamos National Laboratory, Los Alamos, New Mexico, USA.

^b Center for Nonlinear Studies, Los Alamos National Laboratory, Los Alamos, New Mexico 87546

^c Computer, Computational, and Statistical Sciences Division, Los Alamos National Laboratory, Los Alamos, New Mexico, USA.

^d Earth and Environmental Sciences Division, Los Alamos National Laboratory, Los Alamos, New Mexico, USA.

^e Nvidia Corporation, Santa Clara, California, 9505, USA

^f Center for Integrated Nanotechnologies, Los Alamos National Laboratory, Los Alamos, New Mexico 87546

* Correspondence should be addressed to sakibmatin@gmail.com

fields¹ can limit the usability of MLIPs for large scale MD simulations.^{13,43,44}

In this manuscript, we introduce a teacher-student training method for MLIP with a central purpose of building the MLIPs with faster inference and lower memory requirements. The teacher-student training is a class of methods^{45–47} to reduce the inference costs of different ML models and more effectively utilize existing datasets. An initial teacher model is trained and then used to augment the training of a student model that may have faster inference,^{43,47} smaller memory requirements,⁴⁸ or better generalization capacity.⁴⁶ Crucially, this knowledge distillation procedure does not require additional first-principles training data. Instead, auxiliary predictions of the teacher model are used to augment the data used for training of the student model. The innovation in this work is to use the teacher’s local atomic energy predictions as the auxiliary training data. Although these local atomic energies have traditionally been considered a latent feature of the MLIP more,¹¹ the present work highlights that they carry important information. Note that the latent atomic energies provided to the student are far greater in number than the single global QC energy. Thus the student is trained using a significantly larger number of constraints than the teacher. Because the student model will typically have fewer trainable weights than the teacher model, this approach can yield significant gains for inference speed and memory requirements. We also find that the student model can achieve higher-accuracy than the teacher. An overview of our workflow is represented in Fig 1.

2 Methods & Background

We apply the teacher-student training to an MLIP architecture, namely the Hierarchically Interacting Particle Neural Network (HIPNN).^{14,22} HIPNN is a message passing graph neural network used to model atomistic systems,^{22,28} and recent variants incorporate equivariant tensor sensitivity for higher accuracy.¹⁴ The architecture of HIPNN is briefly reviewed in in Sec. 2.1. In Sec. 2.2, we introduce the teacher-student paradigm. Section 2.3 summarizes the training procedure. Sec. 2.4 details the datasets studied. Section 3 contains a systematic exploration of the teacher-student training for the HIPNN model.

2.1 Architecture

HIPNN²² is a message-passing graph neural network⁴⁹ that can map atomic configurations to various chemical properties such as energy,²² forces,¹⁴ dipoles²⁸ etc. Similar to many MLIP architectures, the interaction layers of HIPNN allow for mixing of atomic environments between neighbors via message passing to construct the learnable features.²² The local atomic environment of each atom is initially featurized using atomic number (in HIPNN, as a one-hot encoding, although also common is a random embedding) and passed through several layers along with pair-wise displacement vectors between the neighbors with local cut-off to predict the atom energy ϵ_i for each atom i . Automatic differentiation is used to calculate the forces on each atom from the total molecular energy.

MLIP architectures almost universally infer a local decompo-

sition in their predictions of extensive quantities. In message passing neural network parlance, the readout function is a linear summation over node states. Specifically, in HIPNN, the energy $E[\mathbf{r}_1, \mathbf{r}_2, \dots, \mathbf{r}_N]$ of a configuration, where N is the number of atoms, is decomposed into a sum over local contributions,

$$E \approx \hat{E} = \sum_i^N \epsilon_i. \quad (1)$$

The energy contributions are formed by linear combination of the features (also called embeddings) learned by the neural network. The teacher-student procedure we investigate here depends on the existence of *some* local energy decomposition, but is flexible about its details. For example, our procedure could also work on models such as Allegro that decompose energy into contributions on local bonds.¹⁶

In the original publication,²² HIPNN only used scalar pair-wise distances between neighbors, which captures a subset of the higher-order many-body information contained in the local chemical environment.^{14,41} Subsequently, HIPNN with Tensor Sensitivity¹⁴ utilizes higher order tensor products of the displacement vectors between atoms to construct more informative descriptors. The hyper-parameter l_{\max} corresponds to the highest order tensor used in HIPNN. A weight tying scheme between the different order sensitivity functions leads to only modest increase in number of trainable parameters, thereby reducing the training and evaluation costs, and improving data efficiency.¹⁴ The $l_{\max} = 0$ HIPNN model utilizes only scalar pair-wise distances and coincides with the model developed in original publication.²² In this work we select $l_{\max} = 1$ to allow for vector sensitivity. Other hyper-parameters for the HIPNN models used in this paper are given in Sec. A.1.

2.2 Teacher-Student Training

In the teacher-student training method, a pre-trained teacher model (or models) is used to train a student model to improve speed,^{43,47} memory requirements,⁴⁸ and generalization.⁴⁶ Knowledge Distillation (KD)⁴⁵ is a well known form of teacher-student training. In the original KD publication⁴⁵ auxiliary targets are the teacher model’s predicted relative class probabilities (before the application of the softmax operation in the output layer). The auxiliary targets generated by the teacher contain richer information about the structure of the classes in the dataset. The student models were trained on both the ground truth data and the auxiliary targets and performed better than the control models, which have same architecture as the student but are trained only on the ground truth data. Later works have incorporated deeper architecture dependent knowledge.^{47,48,51} KD has been successfully applied to many different architectures such as CNN,⁵² graph neural networks,⁴⁷ transformers⁴⁸ and more.⁵³ Another variant of the teacher-student training is the “Born Again” (BA) method,⁴⁶ where the student and teacher models have the same architecture, and the student model can surpass the teacher’s accuracy. Multiple teachers can be used to train a single student model to improve performance.^{46,54} Previous works focus on classification tasks on images⁴⁵ and text,⁴⁸

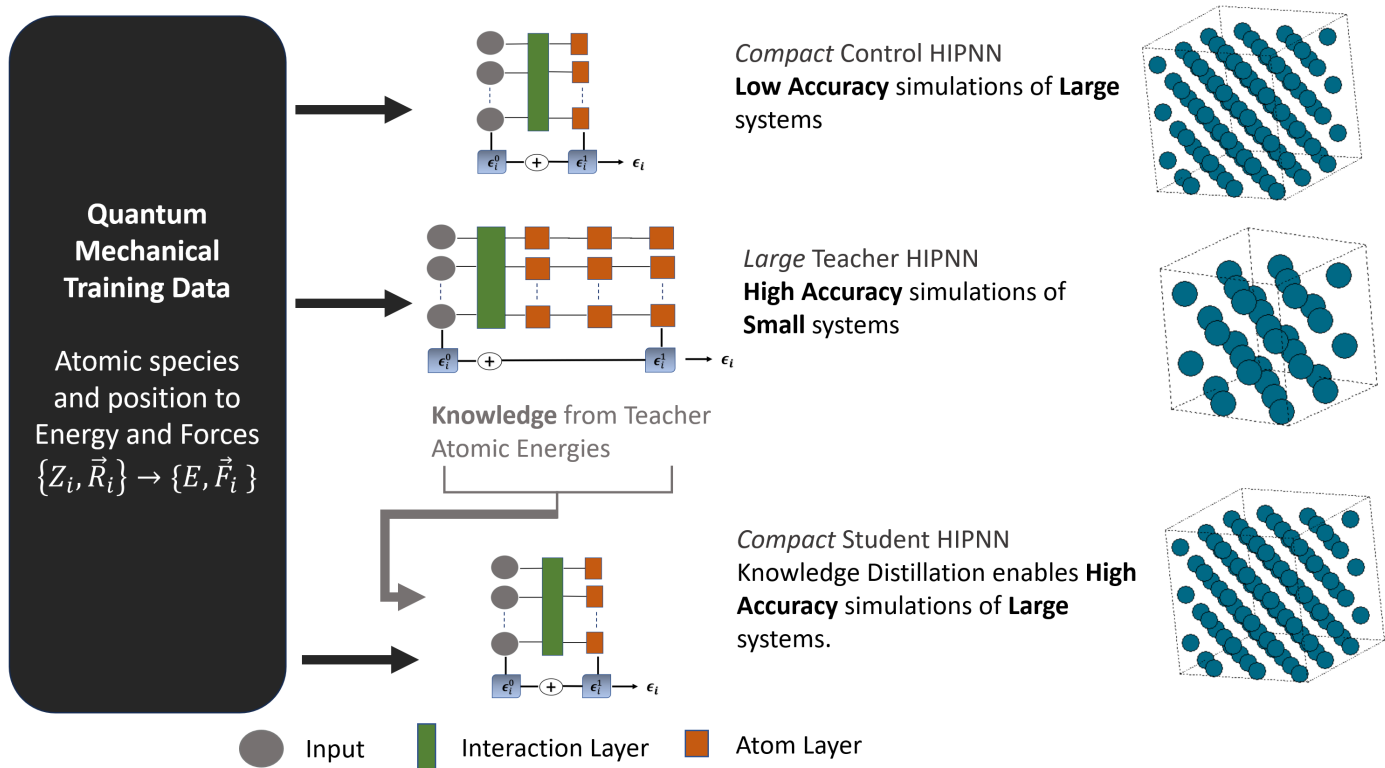


Fig. 1 Teacher-student training for Hierarchically Interacting Particle Neural Network (HIPNN) machine learning inter-atomic potential. A HIPNN model consists of an input node, a message passing interaction layer and feed-forward regression layers called atom layers. The teacher HIPNN is trained on the quantum mechanical energy and forces data, and generates latent knowledge in the form of atomic energies. This augments the student model training to improve the accuracy. The student HIPNN that has fewer trainable weights, which contributes to faster inference and lower memory requirements. The control HIPNNs have the same number of trainable parameters as the student but are trained only on ground truth data. We show that the student models are more accurate than the control models.

and limit applications to regression tasks on graph structured data.⁵⁵

Recently, teacher-student methods have been explored in chemistry for accelerating molecular dynamics⁴³ and material property prediction.⁵⁶ In a related work in Ref. 57, the teacher MLIP (trained on QC ground truth) is used to generate synthetic data by running MD under different conditions. The student model is initially pre-trained on the synthetic data then fine-tuned on the QC ground truth. The atomic energy may provide more fine-grained information than the aggregate configuration energy.^{43,57}

In the first step of our teacher-student method, we train a complex “teacher” MLIP on a QC dataset, which consists of configuration energy and forces on each atom. This teacher MLIP can generate auxiliary targets, namely per-atom energies. Then, we train the student MLIP on the original QC data and auxiliary targets generated by the teacher MLIP. This economical approach does not require any expensive QC calculations beyond the original dataset needed to train the teacher model, nor exhaustive hyper-parameter tuning.

2.3 Training Procedure and Loss Function

We train the teacher model \mathcal{T} on the QC dataset \mathcal{D} , which contains the set of atomic position and species for each configu-

ration and the corresponding energy and the forces per atom, $\mathcal{D} : \{\mathbf{R}_i, Z_i\} \rightarrow \{E, \mathbf{F}_i\}$.

The NN model is trained in a standard manner using stochastic gradient descent on the loss function

$$\mathcal{L}_{\text{Teacher}} = w_E \mathcal{L}_{\text{err}}(\hat{E}, E) + w_F \mathcal{L}_{\text{err}}(\hat{F}, F) + w_{L_2} \mathcal{L}_{L_2} + w_R \mathcal{L}_R. \quad (2)$$

The \mathcal{L}_{L_2} loss term is a regularization of the model weights, which is commonly added to loss functions to reduce over-fitting. The \mathcal{L}_R term, specific to HIPNN, also enhances model stability. The error loss \mathcal{L}_{err} could be any combination of common metrics, but in our case is an equal weighting between root-mean-squared error (RMSE) and mean-absolute error (MAE) losses:

$$\mathcal{L}_{\text{err}}(\hat{V}, V) = \text{RMSE}(\hat{V}, V) + \text{MAE}(\hat{V}, V) \quad (3)$$

where \hat{V} is the model prediction and V is the ground truth target. The weights of each term in the loss are listed in Appendix A.1.

The teacher \mathcal{T} maps the local atomic environments to atomic energies ϵ_i which are summed over to obtain the energy \hat{E} . Although ϵ_i is not directly a physical observable, it nonetheless captures important information about how the local geometry affects the final prediction of the model. Here, we use the teacher MLIP’s atomic energies as the knowledge to be transferred to the student MLIPs.

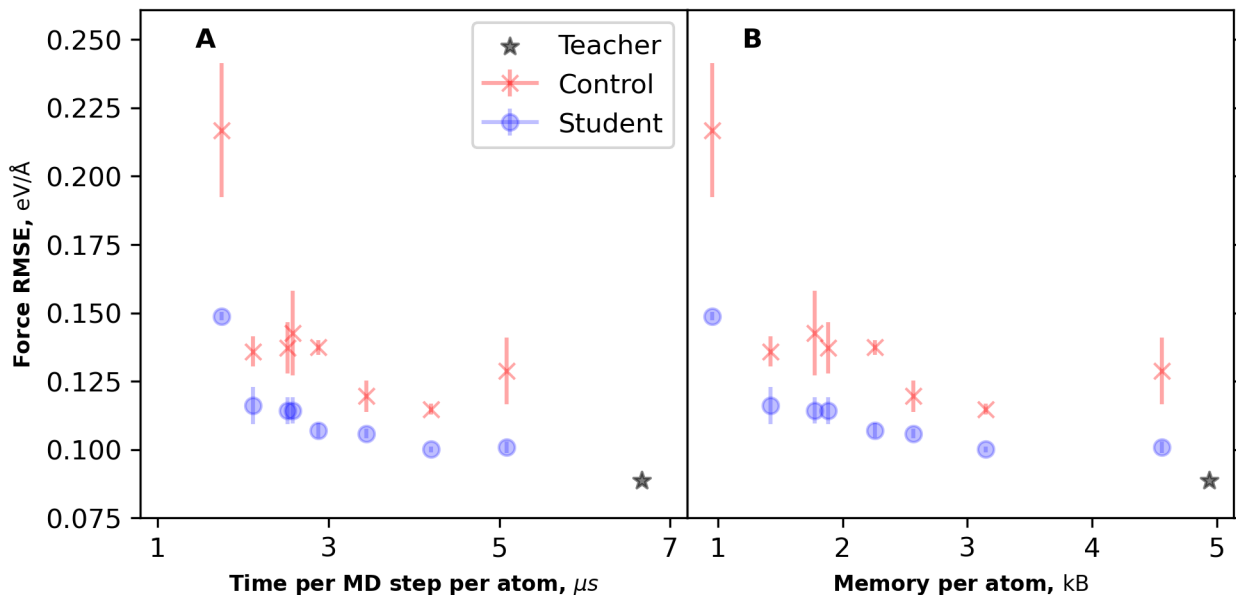


Fig. 2 The student MLIPs are Pareto dominant compared to the control models. The student and control MLIPs are trained on the ANI-1 aluminum dataset.²³ The accuracy metric, force RMSE, is plotted as a function of the efficiency metrics, namely, time per MD step per atom in (A) and memory per atom in (B). The origin of the plots corresponds to the Pareto optimum solution. The MD simulations are run using the ASE⁵⁰ code on a Nvidia A6000 (48GB) GPU.

The atom energy ε_i predictions from \mathcal{T} are used to construct the augmented dataset

$$\tilde{\mathcal{D}}: \{\mathbf{R}_i, Z_i\} \rightarrow \{E, \varepsilon_i^{\mathcal{T}}, \mathbf{F}_i\}. \quad (4)$$

Note that the original dataset \mathcal{D} has the same set of configurations (inputs) as the augmented data $\tilde{\mathcal{D}}$.

We train the student models \mathcal{S} on the augmented dataset $\tilde{\mathcal{D}}$ with the loss function

$$\begin{aligned} \mathcal{L}_{\text{Student}} = & w_E \mathcal{L}_{\text{err}}(\hat{E}, E) + w_F \mathcal{L}_{\text{err}}(\hat{F}, F) + w_A \mathcal{L}_{\text{err}}(\varepsilon^{\mathcal{S}}, \varepsilon^{\mathcal{T}}) \\ & + w_{L_2} \mathcal{L}_{L_2} + w_R \mathcal{L}_R \end{aligned} \quad (5)$$

This captures the notion that the student should learn from the teacher using the loss term $\mathcal{L}_{\text{err}}(\varepsilon^{\mathcal{S}}, \varepsilon^{\mathcal{T}})$ which encourages the partitioning of energy among atomic sites in the student, $\varepsilon^{\mathcal{S}}$, to match that of the teacher, $\varepsilon^{\mathcal{T}}$. We explore student models by varying several architectural parameters of the NN, namely, the layer width n_{feature} , the number of sensitivities function n_d used for the distance embedding, and the number of atom layers used after interaction layers, $n_{\text{atom_layer}}$. To assess the effectiveness of the method, we also train control models \mathcal{C} that have the same architecture as the students \mathcal{S} but are trained only on the dataset \mathcal{D} using $\mathcal{L}_{\mathcal{D}}$; everything else is held constant in these models except for the student-teacher loss. The accuracy of the control models serves as a benchmark to compare the efficacy of the teacher-student training framework.

2.4 Data

We apply our teacher-student workflow on the ANI-1 dataset, which consists of condensed-phase aluminum geometries, with energies and forces calculated using Density Functional Theory (DFT)²³. The dataset was sampled using an automated active learning framework to generate adequate coverage of the configurational space. The dataset consists of about 6,000 DFT calculations (3 electron PBE ultrasoft pseudo-potential, corresponding to the *Al.pbe-n-rrkjus_psl.0.1.UPF* potential in Quantum Espresso⁵⁸). System volumes were periodic, and contain between 55 and 250 aluminum atoms. The thermodynamic conditions span a range of pressures and temperatures. The dataset is available online.⁵⁹

3 Results and Discussion

3.1 Pareto Dominant Student MLIPs

Atomistic simulations require accurate and efficient evaluation of energy and forces. Performing MD at large length and time scales is challenging due to the trade-off between accuracy and efficiency of the inter-atomic potential used in the simulation. MLIPs provide a path to perform MD with QC accuracy at dramatically reduced costs relative to methods that use explicit QC solutions to calculate the forces and energies that are used to evolve the simulation forward in time. Here, we show that the teacher-student methods allow us to further improve the accuracy of MLIPs while keeping the computational costs fixed.

Characterizing the accuracy of inter-atomic potentials in absolute terms is challenging.⁶⁰ Such comparisons should be made against exact numerical solutions or experimental data, which may not be available. The accuracy of MLIPs can be judged

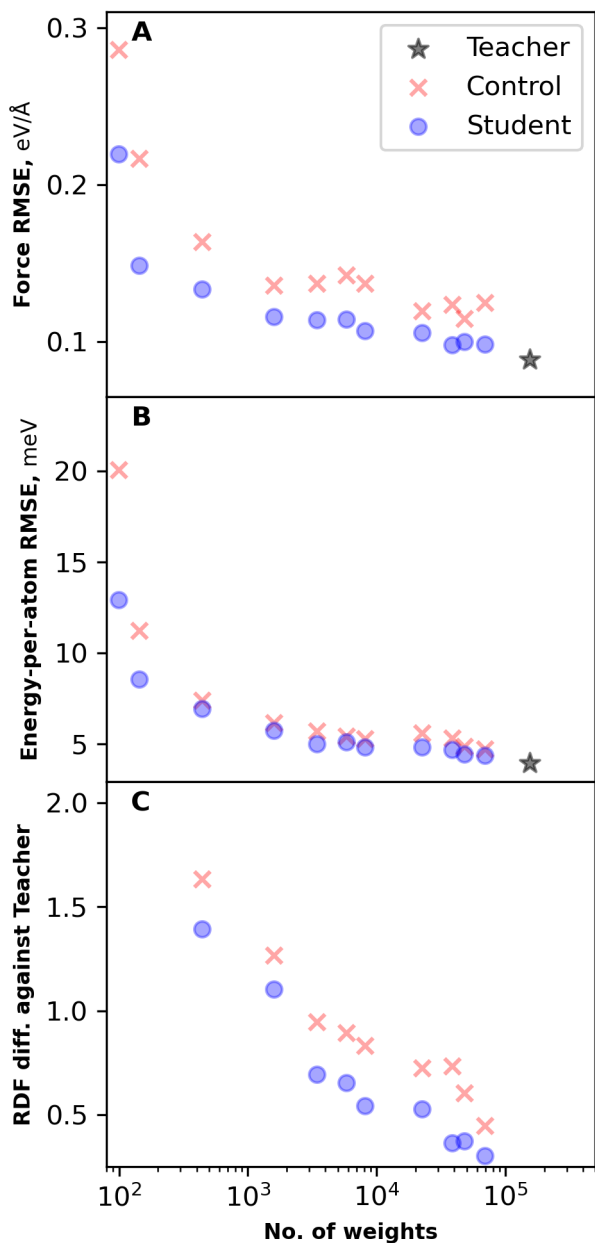


Fig. 3 The student MLIPs are more accurate than the control architectures at the corresponding capacity. The number of trainable weights captures the model capacity. The force RMSE errors and energy per-atom RMSE errors for the training dataset are plotted in panels (A) and (B) respectively. The total absolute error of the radial distribution function (RDF) of the student and control MLIPs compared to the teacher MLIP is shown in panel (C). The error metrics with respect to the training datasets in (A) and (B) show similar trends as the MD-based accuracy metrics in (C).

against held-out test data from the QC calculations used to develop potential. In this section, we use the force root mean squared error (RMSE) as an accuracy measure. We analyze out-of-sample MD-based accuracy metrics in Sec 3.2.

It is also difficult to define an unambiguous metric of efficiency for MLIPs. An informative measure is the time-per-MD step per atom, which is affected by hardware (CPU/GPU memory and processing speeds) and software (MD library, algorithm used for neighbor list construction, etc.). Therefore, in this article, we use a consistent hardware configuration (a single A6000 GPU with 48 GB of storage) and we use the Atomic Simulation Environment⁵⁰ software. We simulate 48,000 atoms at fixed volume and energy (NVE ensemble) with a time step of 1 fs and a simulation time of 1 ps. Additionally, we can characterize the efficiency of MLIPs based on memory requirements. We record the maximum number of atoms that can be simulated on a single A6000 GPU using the ASE software and use it to calculate the average memory-per-atom.

Figure 2 shows the Pareto plot of accuracy (force RMSE) against the time per MD step per atom and maximum atoms per GPU in panels (A) and (B) respectively. The student models are Pareto dominant with respect to the control MLIPs, i.e., for a given cost (MD speed or memory requirement) the student models have higher accuracy than the control models. Each data point is averaged over four MLIPs initialized with different random seeds.

3.2 Accuracy and MLIP Capacity

In Fig. 3, we analyze several metrics of accuracy such as force RMSE errors, energy-per-atom RMSE errors, and radial distribution function (RDF)¹ error as a function of the number of weights of each HIPNN model, which serves as an effective measure of the model capacity. This metric is compelling because it is agnostic to the hardware constraints, such as GPU memory and the choice of MD software. While it is meaningful to compare weights for different variants of a MLIP architecture (HIPNN), care should be taken when making comparisons across different architectures. In Sec. 3.4, we study how the number of weights correlates with the maximum number of atoms per GPU and MD speeds.

The force RMSE errors in panel (A) of Fig 3 indicate a meaningful improvement of the student models compared with the control models, while the energy errors in panel (B) are only minimally improved in the student models. We compute the RDFs of liquid aluminum at 1200 K using the LAVA⁶¹ software, which is a wrapper for LAMMPS.⁵ The reported RDF errors shown in panel (C) for the student and control models are the total absolute errors with respect to the teacher RDFs. This out-of-sample MD test shows a similar trend as the MLIP training/test errors. Note that the energy and forces errors in Fig. 3(A) and (B) respectively are computed with respect to the ground truth training data, whereas the RDF errors in (C) are the differences against the teacher models' MD simulations.

3.3 Learning Dynamics

Learning dynamics (also known as optimization dynamics) characterize how the training or out-of-sample validation error

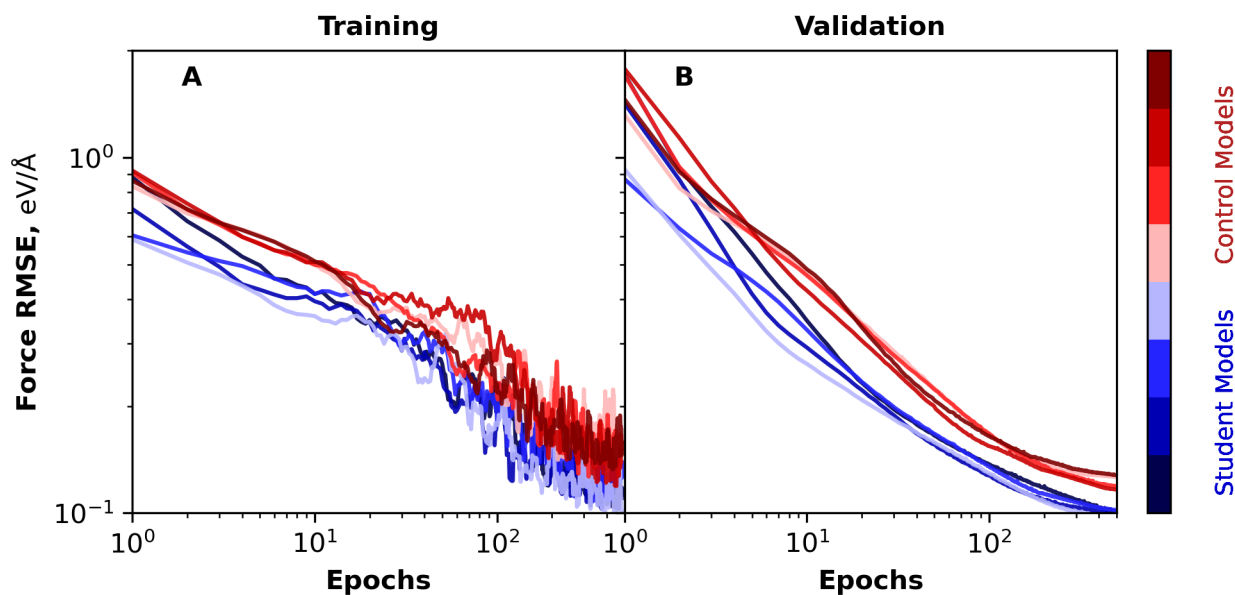


Fig. 4 The student HIPNN MLIP exhibits faster learning dynamics than the control models. Plot of force RMSE errors for the training and validation data splits are shown as a function of epochs for student and control MLIPs in (A) and (B) respectively.

evolves as a function of the training epochs. Here, we analyze learning dynamics of the student and control MLIPs to understand the how the auxiliary targets affect the training. We see in Fig. 4 that the student models’ learning dynamics outperform the control models. loss curves of four different student and control models, which all share the same architecture but different initial weights. Consequently this is reflected in different intercepts, showing that student models train faster than the control models by a roughly constant factor.

3.4 Speed and Scalability

Performing large-scale MD is necessary to address many important scientific questions. While the atomic time-steps are generally of order 1–10 fs, the physical phenomena of interest may span milliseconds or longer and can require billions of atoms. Large-scale MD on modern super-computing clusters relies on the idea of weak scaling,⁵ where the simulation is distributed across many nodes. Due to the high latency of inter-node communications, it is beneficial to fit as many atoms on one node or GPU as possible.

Our work shows that the teacher-student procedure has several benefits for large-scale MD. The light-weight student models require fewer floating point operations for force evaluations. Fig. 5 examines how the number of weights in the network affect the computational cost for large-scale MD in terms of both speed and memory in panels (A) and (B) respectively. The MD is performed using ASE in the NVE ensemble for 1 ps with a time step of 1 fs. Furthermore, we see that the smaller student models can fit more atoms on a single GPU (A6000 48 GB in Fig. 5). The ability to fit more atoms on a single GPU can improve the efficiency of large MD simulations, because inter-node latency can often dominate the computations.⁵

3.5 Student MLIP Surpasses the Teacher

We apply the “Born Again”⁴⁶ teacher-student training to HIPNN. The student and teacher models have the same of trainable weights. We show that student models trained to the ground truth data and the teacher model’s auxiliary outputs and can surpass the teacher by using an loss scheduler.

Initially, we use the static loss function in Eq. 2 to find that student MLIPs achieve comparable errors to the teachers. However, then we utilize a loss scheduler to dynamically update the weights w_A, w_F, w_E during the training as summarized in Table 1 in Appendix A.1. The final weights of the students’ loss function match that of that of the static weights of the teacher MLIP. The student models’ Energy RMSE of 0.37 ± 0.02 eV, and force RMSE of 0.083 ± 0.003 eV/Å is lower than the teacher models errors, energy RMSE of 0.38eV, and force RMSE of 0.092 eV/Å. This shows that the BA teacher-student approach improves the force accuracy by about 10%, which shares the same model architecture and underlying training data.

4 Conclusions and Future work

We show that our teacher-student framework can reduce the inference costs of MLIPs and increase their accuracy without any additional QC data. Our teacher-student training framework improves the Pareto set of error-cost trade-offs for MLIPs. We show that the student MLIPs are Pareto dominant with respect to the control MLIPs. The student MLIPs, trained to the ground truth and teacher’s atomic energies, achieve higher accuracy at the same efficiency (speed and memory requirements) when compared to the control models that were only trained to ground truth. We use both training errors (energy and force RMSEs) as well as MD based metric (RDF errors) to quantify the accuracy of the MLIPs. We find that the force RMSE errors generally cor-

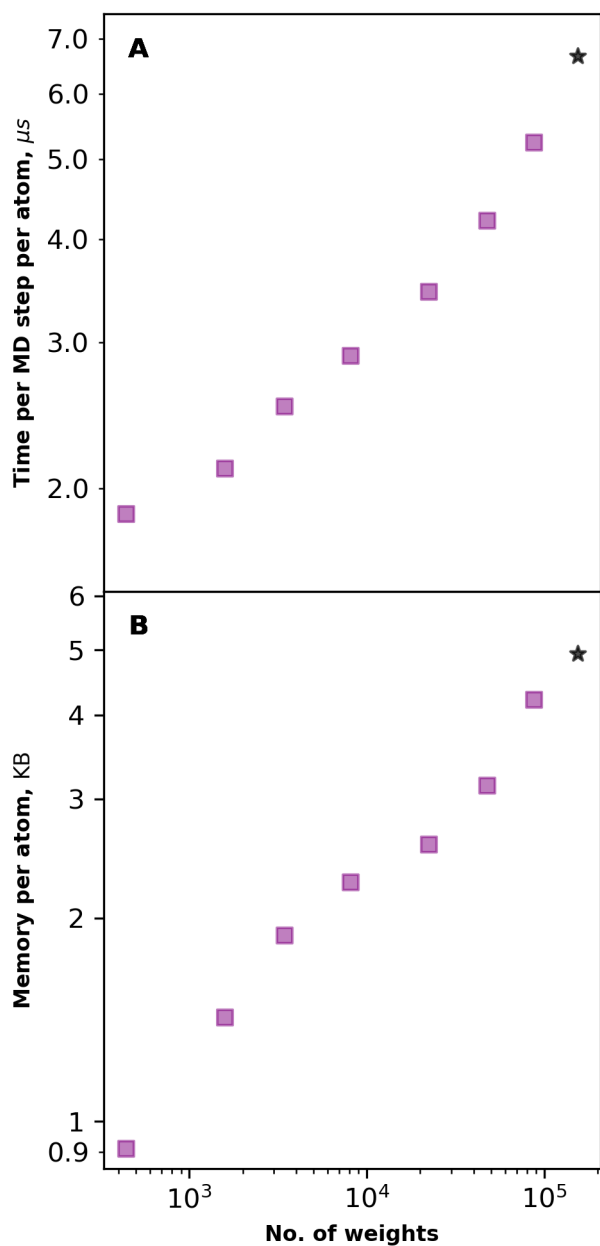


Fig. 5 Inference efficiency as measured by (A) time-per-MD step per atom and (B) memory per atom, versus the number of trainable weights in HIPNN models. Data is collected by running MD simulations using ASE in the NVE ensemble on a single A6000 GPU (48GB) for 10^3 steps.

relate with the MD based metrics, which are costlier to evaluate. Additionally, such MD based metrics require a ground truth, such as ab initio results or experimental data, which may not always be available. Efficiency of MLIPs is also multi-faceted. We use MD speeds and memory-per-atom as effective measures. While MD speed is easy to interpret, it strongly depends on the underlying hardware, MD codes as well as the system under study. The memory-per-atom measure is useful to optimize for large MD simulations, where inter-node communications may dominate. This teacher-student training framework can be readily applied to other MLIPs that decompose the configurational energy into a sum of local contributions.

We used the atomic energies as the knowledge for the teacher-student-training. In the language of message passing graph neural networks, the atom energy is a node level scalar.⁴⁹ We intend to explore node level vectors, such as forces, and edge level properties as knowledge for the teacher-student framework to train across different architectures.⁴³ Additionally, network weights for the interactions layers may be utilized as knowledge for the student. We will also explore using an ensemble of teachers for future work, where the students may be able to leverage the uncertainty associated with the teacher MLIPs' knowledge.

Graph neural networks can be used to predict molecular properties beyond just energy and forces such as charges,^{29,62} dipoles,²⁸ and other properties.¹¹ We will explore cross-modal teacher-student training frameworks to combine teacher models with different specialized tasks to train generalist student MLIPs. This will be an important step towards foundation models for chemistry with broad applicability.

A Training Details

A.1 Hyper-Parameters

We use HIPNN models with 1 interaction layer. The teacher models use 4 atom layers (feed-forward layers) with a width of 128. The student (and control) models have between 1 and 4 atom layers with width between 12 and 128. All models have maximum tensor sensitivity order set at $l_{\max} = 1$. For the sensitivity functions which parameterize the interaction layer, radial basis functions are used with a soft-min cutoff of 1.5 \AA , the soft maximum cutoff of 7.0 \AA , and hard maximum cutoff of 7.5 \AA . The teacher model uses 40 basis functions. For the student (and control) MLIPs, we use between 8 and 40 sensitivity functions. The soft-min cut-off corresponds to the inner cut-off at very short distances. The hard maximum cut-off corresponds to the long distance cut-off. The soft maximum cutoff is set to a value smaller than the hard-dist cutoff to ensure a smooth truncation of the sensitivity functions. Note that we are using the naming conventions for the hyper-parameters in the HIPNN GitHub Repository,⁶³ which differs slightly from the original HIPNN publication.²²

We summarize the weights corresponding the loss function in Eq. 2. $W_{L_2} = 10^{-6}$ and $W_R = 0.01$ is common to the teacher, student and control models. $W_E = 1$ and $W_F = 10$ for the teacher and control MLIPs. Lastly, we used $W_E = 1$, $W_F = 30$ and $W_A = 100$ for the student models. For the BA training, we use a loss schedule

with weights given in Table 1.

We used the Adam Optimizer, with an initial learning rate of 0.001, which is halved with a patience of 30 epochs. The termination patience is 50 epochs.

Table 1 Loss Scheduler for Student MLIPs for the Born-Again method of teacher-student training in Sec. 3.5

Epoch	w_A	w_F	w_E
1	200	75	0.0
200	160	63	0.2
250	120	51	0.4
300	80	39	0.6
350	40	27	0.8
400	0	15	1

Conflicts of interest

There are no conflicts to declare.

Data availability

The HIPNN^{14,22} MLIP is implemented in an open-source PyTorch-based software package called hippynn which is available for download.⁶³

We use an aluminum dataset published in Ref. 23 which is available for download.⁵⁹

Acknowledgements

This work was supported by the United States Department of Energy (US DOE), Office of Science, Basic Energy Sciences, Chemical Sciences, Geosciences, and Biosciences Division under Triad National Security, LLC (“Triad”) contract grant no. 89233218CNA000001 (FWP: LANLE3F2). We acknowledge support from the Los Alamos National Laboratory (LANL) Directed Research and Development funds (LDRD). This research was performed in part at the Center for Nonlinear Studies (CNLS) at LANL. This research used resources provided by the Darwin testbed at LANL which is funded by the Computational Systems and Software Environments subprogram of LANL’s Advanced Simulation and Computing program.

Notes and references

- 1 Allen, Michael P. and Tildesley, Dominic J., *Computer Simulation of Liquids*, Oxford university press, 2017.
- 2 M. E. Tuckerman and G. J. Martyna, *The Journal of Physical Chemistry B*, 2000, **104**, 159–178.
- 3 M. O. Steinhauser and S. Hiermaier, *International Journal of Molecular Sciences*, 2009, **10**, 5135–5216.
- 4 M. De Vivo, M. Masetti, G. Bottegoni and A. Cavalli, *Journal of Medicinal Chemistry*, 2016, **59**, 4035–4061.
- 5 A. P. Thompson, H. M. Aktulga, R. Berger, D. S. Bolintineanu, W. M. Brown, P. S. Crozier, P. J. in’t Veld, A. Kohlmeyer, S. G. Moore, T. D. Nguyen *et al.*, *Computer Physics Communications*, 2022, **271**, 108171.
- 6 J. Jung, W. Nishima, M. Daniels, G. Bascom, C. Kobayashi, A. Adedoyin, M. Wall, A. Lappala, D. Phillips, W. Fischer, C.-S. Tung, T. Schlick, Y. Sugita and K. Y. Sanbonmatsu, *Journal of Computational Chemistry*, 2019, **40**, 1919–1930.
- 7 A. Szabo and N. S. Ostlund, *Modern Quantum Chemistry: Introduction to Advanced Electronic Structure Theory*, Courier Corporation, 2012.
- 8 K. Burke, *J. Chem. Phys.*, 2012, **136**, 150901.
- 9 Y. Zuo, C. Chen, X. Li, Z. Deng, Y. Chen, J. Behler, G. Csányi, A. V. Shapeev, A. P. Thompson, M. A. Wood and S. P. Ong, *The Journal of Physical Chemistry A*, 2020, **124**, 731–745.
- 10 V. L. Deringer, A. P. Bartók, N. Bernstein, D. M. Wilkins, M. Cerriotti and G. Csányi, *Chem. Rev.*, 2021, **121**, 10073–10141.
- 11 N. Fedik, R. Zubatyuk, M. Kulichenko, N. Lubbers, J. S. Smith, B. Nebgen, R. Messerly, Y. W. Li, A. I. Boldyrev, K. Barros, O. Isayev and S. Tretiak, *Nat. Rev. Chem.*, 2022, **6**, 653–672.
- 12 M. Kulichenko, J. S. Smith, B. Nebgen, Y. W. Li, N. Fedik, A. I. Boldyrev, N. Lubbers, K. Barros and S. Tretiak, *The Journal of Physical Chemistry Letters*, 2021, **12**, 6227–6243.
- 13 O. T. Unke, S. Chmiela, H. E. Sauceda, M. Gastegger, I. Poltavsky, K. T. Schütt, A. Tkatchenko and K.-R. Müller, *Chemical Reviews*, 2021, **121**, 10142–10186.
- 14 M. Chigaev, J. S. Smith, S. Anaya, B. Nebgen, M. Bettencourt, K. Barros and N. Lubbers, *The Journal of Chemical Physics*, 2023, **158**, 184108.
- 15 J. Behler, *The Journal of Chemical Physics*, 2016, **145**, 170901.
- 16 H. Ibayashi, T. M. Razakh, L. Yang, T. Linker, M. Olguin, S. Hattori, Y. Luo, R. K. Kalia, A. Nakano, K.-i. Nomura and P. Vashishta, International Conference on High Performance Computing, 2023, pp. 223–239.
- 17 J. Behler and M. Parrinello, *Phys. Rev. Lett.*, 2007, **98**, 146401.
- 18 A. P. Bartók, M. C. Payne, R. Kondor and G. Csányi, *Phys. Rev. Lett.*, 2010, **104**, 136403.
- 19 M. Rupp, A. Tkatchenko, K.-R. Müller and O. A. von Lilienfeld, *Phys. Rev. Lett.*, 2012, **108**, 058301.
- 20 J. S. Smith, O. Isayev and A. E. Roitberg, *Chemical Science*, 2017, **8**, 3192–3203.
- 21 K. T. Schütt, H. E. Sauceda, P.-J. Kindermans, A. Tkatchenko and K.-R. Müller, *The Journal of Chemical Physics*, 2018, **148**, 241722.
- 22 N. Lubbers, J. S. Smith and K. Barros, *The Journal of Chemical Physics*, 2018, **148**, 241715.
- 23 J. S. Smith, B. Nebgen, N. Mathew, J. Chen, N. Lubbers, L. Burakovsky, S. Tretiak, H. A. Nam, T. Germann, S. Fensin and K. Barros, *Nat. Commun.*, 2021, **12**, 1–13.
- 24 D. P. Kovács, C. V. D. Oord, J. Kucera, A. E. A. Allen, D. J. Cole, C. Ortner and G. Csányi, *Journal of Chemical Theory and Computation*, 2021, **17**, 7696–7711.
- 25 S. Bätzner, A. Musaelian, L. Sun, M. Geiger, J. P. Mailoa, M. Kornbluth, N. Molinari, T. E. Smidt and B. Kozinsky, *Nat. Commun.*, 2022, **13**, 1–11.
- 26 O. T. Unke and M. Meuwly, *J. Chem. Theory Comput.*, 2019, **15**, 3678–3693.
- 27 K. Yao, J. E. Herr, D. W. Toth, R. Mckintyre and J. Parkhill, *Chem. Sci.*, 2018, **9**, 2261–2269.
- 28 A. E. Sifain, N. Lubbers, B. T. Nebgen, J. S. Smith, A. Y. Lokhov, O. Isayev, A. E. Roitberg, K. Barros and S. Tretiak, *The Journal of Physical Chemistry Letters*, 2018, **9**, 4495–4501.

- 29 T. W. Ko, J. A. Finkler, S. Goedecker and J. Behler, *Nature Communications*, 2021, **12**, 398.
- 30 T. W. Ko, J. A. Finkler, S. Goedecker and J. Behler, *Journal of Chemical Theory and Computation*, 2023, 3567–3579.
- 31 M. Eckhoff, K. N. Lausch, P. E. Blöchl and J. Behler, *The Journal of Chemical Physics*, 2020, **153**, 164107.
- 32 N. T. P. Tu, N. Rezajooei, E. R. Johnson and C. N. Rowley, *Digital Discovery*, 2023, **2**, 718–727.
- 33 J. A. Rackers, L. Tecot, M. Geiger and T. E. Smidt, *Machine Learning: Science and Technology*, 2023, **4**, 015027.
- 34 E. Shinkle, A. Pachalieva, R. Bahl, S. Matin, B. Gifford, G. T. Craven and N. Lubbers, *Journal of Chemical Theory and Computation*, 2024, **20**, 10524–10539.
- 35 S. Magedov, C. Koh, W. Malone, N. Lubbers and B. Nebgen, *Journal of Applied Physics*, 2021, **129**, 064701.
- 36 I. Batatia, P. Benner, Y. Chiang, A. M. Elena, D. P. Kovács, J. Riebesell, X. R. Advincula, M. Asta, W. J. Baldwin, N. Bernstein *et al.*, *arXiv preprint arXiv:2401.00096*, 2023.
- 37 A. E. Allen, N. Lubbers, S. Matin, J. Smith, R. Messerly, S. Tretiak and K. Barros, *npj Computational Materials*, 2024, **10**, 154.
- 38 D. Zhang, H. Bi, F.-Z. Dai, W. Jiang, X. Liu, L. Zhang and H. Wang, *npj Computational Materials*, 2024, **10**, 94.
- 39 A. Jain, S. P. Ong, G. Hautier, W. Chen, W. D. Richards, S. Dacek, S. Cholia, D. Gunter, D. Skinner, G. Ceder and K. A. Persson, *APL Materials*, 2013, **1**, 011002.
- 40 R. Bommasani, D. A. Hudson, E. Adeli, R. Altman, S. Arora, S. von Arx, M. S. Bernstein, J. Bohg, A. Bosselut, E. Brunskill *et al.*, *arXiv preprint arXiv:2108.07258*, 2021.
- 41 I. Batatia, D. P. Kovacs, G. Simm, C. Ortner and G. Csányi, *Advances in Neural Information Processing Systems*, 2022, **35**, 11423–11436.
- 42 Sriram, Anuroop and Das, Abhishek and Wood, Brandon M. and Goyal, Siddharth and Zitnick, C. Lawrence, *arXiv preprint arXiv:2203.09697*, 2022.
- 43 F. E. Kelvinius, D. Georgiev, A. P. Toshev and J. Gasteiger, *arXiv preprint arXiv:2306.14818*, 2023.
- 44 S. R. Xie, M. Rupp and R. G. Hennig, *npj Computational Materials*, 2023, **9**, 162.
- 45 G. Hinton, O. Vinyals and J. Dean, NIPS Deep Learning and Representation Learning Workshop, 2015.
- 46 T. Furlanello, Z. Lipton, M. Tschannen, L. Itti and A. Anandkumar, International Conference on Machine Learning, 2018, pp. 1607–1616.
- 47 Y. Yang, J. Qiu, M. Song, D. Tao and X. Wang, Proceedings of the IEEE/CVF Conference on Computer Vision and Pattern Recognition, 2020, pp. 7074–7083.
- 48 V. Sanh, L. Debut, J. Chaumond and T. Wolf, *arXiv preprint arXiv:1910.01108*, 2019.
- 49 A. Duval, S. V. Mathis, C. K. Joshi, V. Schmidt, S. Miret, F. D. Malliaros, T. Cohen, P. Liò, Y. Bengio and M. Bronstein, *arXiv preprint arXiv:2312.07511*, 2023.
- 50 A. Hjorth Larsen, J. Jørgen Mortensen, J. Blomqvist, I. E. Castelli, R. Christensen, M. Dułak, J. Friis, M. N. Groves, B. Hammer, C. Hargus, E. D. Hermes, P. C. Jennings, P. Bjerre Jensen, J. Kermode, J. R. Kitchin, E. Leonhard Kolsbjerg, J. Kubal, K. Kaasbjerg, S. Lysgaard, J. Bergmann Maronsson, T. Maxson, T. Olsen, L. Pastewka, A. Peterson, C. Rossgaard, J. Schiøtz, O. Schütt, M. Strange, K. S. Thygesen, T. Vegge, L. Vilhelmsen, M. Walter, Z. Zeng and K. W. Jacobsen, *J. Phys.: Condens.Matter*, 2017, **29**, 273002.
- 51 J. Gou, B. Yu, S. Maybank and D. Tao, *arXiv preprint arXiv:2006.05525*, 2020.
- 52 K. Xu, L. Rui, Y. Li and L. Gu, European conference on computer vision, 2020, pp. 664–680.
- 53 Gou, Jianping and Yu, Baosheng and Maybank, Stephen J. and Tao, Dacheng, *International Journal of Computer Vision*, 2021, **129**, 1789–1819.
- 54 Y. Chebotar and A. Waters, Interspeech, 2016, pp. 3439–3443.
- 55 Q. Xu, Z. Chen, M. Ragab, C. Wang, M. Wu and X. Li, *Neurocomputing*, 2022, **485**, 242–251.
- 56 D. Zhu, Z. Xin, S. Zheng, Y. Wang and X. Yang, *Journal of Chemical Theory and Computation*, 2024.
- 57 Gardner, John L. A. and Faure Beaulieu, Zoé and Deringer, Volker L., *Digital Discovery*, 2023.
- 58 P. Giannozzi, O. Andreussi, T. Brumme, O. Bunau, M. B. Nardelli, M. Calandra, R. Car, C. Cavazzoni, D. Ceresoli, M. Cococcioni, N. Colonna, I. Carnimeo, A. D. Corso, S. de Gironcoli, P. Delugas, R. A. DiStasio, A. Ferretti, A. Floris, G. Fratesi, G. Fugallo, R. Gebauer, U. Gerstmann, F. Giustino, T. Gorni, J. Jia, M. Kawamura, H.-Y. Ko, A. Kokalj, E. Küçükbenli, M. Lazzeri, M. Marsili, N. Marzari, F. Mauri, N. L. Nguyen, H.-V. Nguyen, A. O. de-la Roza, L. Paulatto, S. Poncé, D. Rocca, R. Sabatini, B. Santra, M. Schlipf, A. P. Seitsonen, A. Smogunov, I. Timrov, T. Thonhauser, P. Umari, N. Vast, X. Wu and S. Baroni, *Journal of physics: Condensed matter*, 2017, **29**, 465901.
- 59 ANI-AL data and model GitHub repository. <https://github.com/atomistic-ml/ani-al>.
- 60 Y. Liu, X. He and Y. Mo, *arXiv preprint arXiv:2306.11639*, 2023.
- 61 K. Dang, J. Chen, B. Rodgers and S. Fensin, *Computer Physics Communications*, 2023, **286**, 108667.
- 62 B. Nebgen, N. Lubbers, J. S. Smith, A. E. Sifain, A. Lokhov, O. Isayev, A. E. Roitberg, K. Barros and S. Tretiak, *Journal of Chemical Theory and Computation*, 2018, **14**, 4687–4698.
- 63 The hippynn package - a modular library for atomistic machine learning with PyTorch, available online: <https://github.com/lanl/hippynn>.

Knowledge Distillation for Machine Learning Inter-atomic potentials (MLIPs)

